

Molecular Biophysics:
**Predicting enzyme adsorption to lignin
films by calculating enzyme surface
hydrophobicity**

Deanne W. Sammond, John M. Yarbrough,
Elisabeth Mansfield, Yannick J.. Bomble,
Sarah E. Hobdey, Stephen R. Decker, Larry E.
Taylor, Michael G. Resch, Joseph J. Bozell,
Michael E. Himmel, Todd B. Vinzant and
Michael F. Crowley
J. Biol. Chem. published online May 29, 2014

MOLECULAR
BIOPHYSICS

PROTEIN STRUCTURE
AND FOLDING

Access the most updated version of this article at doi: [10.1074/jbc.M114.573642](https://doi.org/10.1074/jbc.M114.573642)

Find articles, minireviews, Reflections and Classics on similar topics on the [JBC Affinity Sites](#).

Alerts:

- [When this article is cited](#)
- [When a correction for this article is posted](#)

[Click here](#) to choose from all of JBC's e-mail alerts

This article cites 0 references, 0 of which can be accessed free at
<http://www.jbc.org/content/early/2014/05/29/jbc.M114.573642.full.html#ref-list-1>

Predicting enzyme adsorption to lignin films by calculating enzyme surface hydrophobicity

Deanne W. Sammond^{§,1}, John M. Yarbrough^{§,1}, Elisabeth Mansfield[¶], Yannick J. Bomble[§], Sarah E. Hobdey[§], Stephen R. Decker[§], Larry E. Taylor[§], Michael G. Resch^{§,#}, Joseph J. Bozell[†], Michael E. Himmel[§], Todd B. Vinzant[§], and Michael F. Crowley[§]

[§]From the Biosciences Center and [#]National Bioenergy Center, National Renewable Energy Laboratory, Golden, Colorado 80401

[¶]Applied Chemicals and Materials Division, National Institute for Standards and Technology, Boulder, Colorado 80305

[†]Center for Renewable Carbon, Center for the Catalytic Conversion of Biomass (C3Bio), University of Tennessee, Knoxville, Tennessee 37917, United States

¹These authors contributed equally to this work.

*Running title: Hydrophobic clusters predict level of enzyme adsorption to lignin

To whom correspondence should be addressed: Michael F. Crowley, Biosciences Center, National Renewable Energy Laboratory, 16253 Denver West Parkway, Golden, CO 80401, Tel.: (303) 384-6345; Fax: (303) 384-7752; E-mail: Michael.Crowley@nrel.gov

Keywords: cellulase; glycoside hydrolases; protein chemistry; protein engineering; enzyme inhibitors; lignin; hydrophobic interaction

Background: Lignin is a plant cell wall polymer that inhibits enzymatic saccharification of polysaccharides for the production of biofuel.

Results: The adsorption of enzymes to lignin surfaces correlates to solvent exposed hydrophobic clusters.

Conclusion: Hydrophobicity, not surface charge, identifies proteins that preferentially adsorb to lignin.

Significance: The method could be used to design improved cellulase cocktails to lower the cost of biofuel production.

The inhibitory action of lignin on cellulase cocktails is a major challenge to the biological saccharification of plant cell wall polysaccharides. While the mechanism remains unclear, hydrophobic interactions between enzymes and lignin are hypothesized to drive adsorption. Here we evaluate the role of hydrophobic interactions in enzyme-lignin

binding. The hydrophobicity of the enzyme surface was quantified using an estimation of the clustering of nonpolar atoms, identifying potential interaction sites. The adsorption of enzymes to lignin surfaces, measured using the quartz crystal microbalance, correlates to the hydrophobic cluster scores. Further, these results suggest a minimum hydrophobic cluster size for a protein to preferentially adsorb to lignin. The impact of electrostatic contribution was ruled out by comparing the isoelectric point (pI) values to the adsorption of proteins to lignin surfaces. These results demonstrate the ability to predict enzyme-lignin adsorption and could potentially be used to design improved cellulase cocktails, thus lowering the overall cost of biofuel production.

Currently the cost of enzymes required for enzymatic digestion of biomass is a significant part of the total cost of producing lignocellulosic fuel; a recent techno-economic estimation attributes a cost of \$1.47/gallon of ethanol produced from corn stover to enzyme production (1). The inhibitory effect of lignin is known to

decrease the performance of cellulase cocktails and results in the need for high enzyme loadings. Nonproductive adsorption of cellulases to lignin is hypothesized to be a source of inhibition, yet the mechanisms driving enzyme adsorption have not been elucidated. This study is aimed at understanding the factors contributing to lignin inhibition and proposing solutions to advance the development of enzyme cocktails by reducing non-specific binding to lignin.

Lignin is a polymer of cross-linked phenylpropane units, conferring hydrophobicity, structural rigidity and microbial resistance to plant cell walls. The physical properties of lignin, which can vary among different plant sources and result from different pretreatment methods, can influence enzyme adsorption capacity. The hydrophilic carboxylic acid functionality in lignin samples correlates with enzymatic hydrolysis of lignocellulosic substrates, suggesting some chemical properties of lignin may reduce enzyme adsorption to lignin (2). Attempts to genetically engineer plants for altered lignin biosynthesis can result in the incorporation of unusual phenylpropane units, such as coniferaldehyde, leading to an increase in hydrophobicity (3). This increased hydrophobicity in genetically engineered plants has led to a decrease in digestibility of the cell wall. Thus, while the mechanism of enzymatic inhibition by lignin is not fully understood, hydrophobicity appears to have a strong role.

Research of enzyme adsorption to lignin has focused on several mechanisms. The role of electrostatic interactions was investigated by comparing enzyme adsorption and protein pI values, but the results are inconclusive as both positively and negatively charged proteins were found to adsorb to lignin (4). The role of the carbohydrate-binding module (CBM), found in many cellulase enzymes and important for targeting enzyme to substrate, was shown to enhance enzyme adsorption to lignin (5). However, another study utilizing a cocktail of cellulase enzymes found β -glucosidase, which does not have a CBM, preferentially adsorbs to lignin (6).

Enzymatic hydrolysis of lignocellulosic biomass can be enhanced by the inclusion of various protein and chemical additives. Bovine serum albumin (BSA) has been used as a non-enzymatic protein additive to enhance glucose

yields in enzymatic hydrolysis (7,8), based on its propensity to non-specifically bind hydrophobic steroid hormones, hemin and fatty-acids (9). A study assessing exposed hydrophobic regions of 112 soluble, monomeric proteins identifies BSA near the top for the amount of exposed hydrophobic surface regions (10). Yang et al. showed that BSA adsorbs more strongly to pretreated corn stover, which contains both cellulose and lignin, than to model cellulose (7). Additionally, an enhancement of enzymatic hydrolysis upon the addition of BSA is seen for pretreated corn stover but not for model cellulose. The results imply that adsorption to lignin is the mechanism for inhibition and that added BSA binds to lignin preventing cellulase binding.

Similar enhancements to enzymatic hydrolysis of lignocellulosic biomass have been seen upon the addition of non-ionic surfactants such as Tween detergents, polyethylene glycol 4000 or dodecylbenzene sulfonic acid (11-15). Numerous mechanisms could lead to the enhancement effect including [1] increasing protein stability, [2] altering lignin structure and [3] altering enzyme-lignin interaction. Addressing these proposed mechanisms, Eriksson et al. found surfactants have very little effect on the thermal stability of *Trichoderma reesei* Cel7A but did enhance the hydrolysis of lignocellulose while not improving model cellulose hydrolysis. These results coincided with a decrease in enzyme adsorption to lignin (12). These observations are in agreement with BSA results, and support the role of surfactants in attenuating nonproductive enzyme adsorption to lignin. Furthermore, the results support the hypothesis that enzymes interact with lignin through a hydrophobic mechanism.

Although lignin adsorption is likely to have other dependencies, if hydrophobicity is a significant contributor then hydrophobic surface properties could determine how strongly various enzymes adsorb to lignin. Additionally, protein engineers might have a clear and rational approach to mitigate these undesired interactions. Lijnzaad et al. developed a method to delineate contiguous hydrophobic patches on a protein surface (16). Briefly, all nonpolar atoms with nonzero solvent accessible surface area (SASA) are assigned to be nodes on a graph, and edges are placed between nodes if there is exposed overlap between atoms.

Jacek et al. incorporated a similar method into the protein design software, Rosetta, adding a scoring function specifically designed to identify larger hydrophobic patches (17). The Rosetta hydrophobic patch score works by assigning a score to each identified patch, with scores increasing exponentially with increasing patch size.

Here we take a systematic approach to evaluate the surface properties of a select set of proteins for comparison to measured adsorption to lignin surfaces. The method developed by Jacek et al. is used to rank-order each protein by degree of surface hydrophobicity. Then the strength of the interactions between enzymes and lignin films is evaluated using quartz crystal microbalance with dissipation monitoring (QCM-D). QCM-D enables real-time measurements of enzyme adsorption to substrate films. Comparing surface properties for the studied set of enzymes to adsorption information provides information on how well the hydrophobic patch score predicts degree of binding. We describe enzyme interactions with lignin isolated from switchgrass via an organosolv process as an example of a biomass pretreatment process potentially useful in biofuel production.

EXPERIMENTAL PROCEDURES

Hydrophobic surface analysis - Surface properties of individual enzymes were evaluated using the protein design software, Rosetta (18,19). Rosetta was used to identify and score clusters of hydrophobic atoms, referred to as hydrophobic patches (17). Additionally, hydrophobic and hydrophilic solvent accessible surface area was computed for each structure using VADAR (Volume, Area, Dihedral Angle Reporter) (20). The molecular weight for each protein was computed based on the amino acid sequence using the ExPASy ProtParam tool (21).

Enzyme structures - Structural analysis using Rosetta requires modeled or experimentally determined structures. Experimentally determined protein structures were obtained from the protein databank (22), including the following: Bovine Serum Albumin (PDB 4f5s) (23), the catalytic domains of *Acidothermus cellulolyticus* Endocellulase E1 (Cel5A, PDB 1c0d) (24), *Trichoderma reesei* Cellobiohydrolase I (Cel7A, PDB 1cel) (25), the family 1 carbohydrate binding

module of *Trichoderma reesei* Cel7A (CBM1, PDB 1cbh) (26), *Thermomyces lanuginosus* Endo-1,4- β -Xylanase (XynA, PDB 1yna) (27), *Trichoderma reesei* Eno-1,4- β -Xylanase (XynII, PDB 1enx) (28), and *Trichoderma reesei* Acetyl Xylan Esterase (AxeI, PDB 1qoz) (29).

Homology models were used for proteins or individual domains lacking an experimentally determined structure. Alpha-L-arabinofuranosidase B (Abfb) from *Aspergillus niger* shares 98% sequence identity with *Aspergillus kawachii* IFO4308 AbfB, which has an experimentally determined structure (PDB 1wd3) (30). A homology model was obtained from the SWISS-MODEL Repository based on 1wd3 (31). The *Trichoderma reesei* AxeI CBM1 shares 69.5% sequence identity with the Cel7A CBM1. The AxeI CBM1 sequence was modeled onto the *Trichoderma reesei* Cel7A CBM1 structure (PDB 1cbh) using Rosetta. The *Aspergillus niger* β -glucosidase (BgII) shares 84% sequence identity with the *Aspergillus aculeatus* β -glucosidase, which has an experimentally determined structure (PDB 4iib) (32). A sequence alignment was generated using MacVector (33) and the sequence for *Aspergillus niger* was threaded onto 4iib using Rosetta. Missing coordinates were built using SWISS-MODEL homology modeling tools (31).

Enzymes - BSA from Pierce was purchased from Thermo Scientific (Rockford, IL). *Aspergillus niger* β -glucosidase was purchased from Megazymes (Wicklow, Ireland). *Trichoderma reesei* XynII was purchased from Hampton Research (Aliso Viejo, CA). All purchased enzymes were desalted on HiPrep Desalting columns (GE Lifesciences, Piscataway, NJ) into 20mM sodium acetate pH 5.0, 100mM sodium chloride buffer.

Thermomyces lanuginosus XynA was purchased from SigmaAldrich (St. Louis, MO) packaged as Pentopan® from Novozymes (34). Purification of XynA consisted of solubilizing the protein in 20 mM Tris buffer- pH 8.0 followed by centrifugation to remove the protein from the flour (Pentopan® is a baking additive) and subjecting the clarified supernatant to anion exchange chromatography on a Source15Q 10/100 Tricorn chromatography column (GE Lifesciences) with a 0.0 to 1.0 M sodium chloride gradient in 20 mM Bis-Tris buffer pH 8.0. Active fractions were pooled, concentrated by 5 kDa Vivaflow spin

concentrators (Millipore), and subjected to size-exclusion chromatography on a 26/60 Superdex 75 column in 20 mM sodium acetate pH 5.0, 100 mM sodium chloride.

Acidothermus cellulolyticus endoglucanase E1 (Cel5A) was expressed in *Escherichia coli* BL21 as a truncated gene (CBM and linker delete) with a Y to G mutation at sequence position 245 (E1cdY245G). The protein was purified as described previously (35).

Trichoderma reesei Axel was expressed in *Aspergillus awamori* and purified using combinations of hydrophobic interaction, anion exchange, and size-exclusion FPLC as described previously (36).

α -L-arabinofuranosidase B (AbfB) from *Aspergillus niger* was expressed in and purified from *Aspergillus awamori* grown in CM-maltose medium at 30°C, with shaking, for 6 days. Culture broth was filtered stepwise through Miracloth, 2.7 μ m, 1.5 μ m, 0.7 μ m, and 0.45 μ m filters, then concentrated and buffer exchanged into 20 mM Bis-Tris pH 6.8 through a PES filter with 5 kDa cut-off (Pall Life Sciences). Buffer exchanged broth proteins were separated by anion exchange using HiTrap Q Sepharose HP column (GE Lifesciences) with a 0.0 to 1.0 M sodium chloride gradient in 20 mM Bis-Tris pH 6.8. AbfB was followed by activity on o-nitrophenyl- α -L-arabinofuranoside (Sigma Life Science) and molecular weight as determined by SDS-Page on a 4 to 12% polyacrylamide gradient gel (Life Technologies, Grand Island, NY). AbfB fractions were pooled and diluted in high salt buffer (4.0 M (NH₄)₂SO₄ 20 mM Bis-Tris pH 6.8) to a final salt concentration of 2.0 M (NH₄)₂SO₄ for purification by HiTrap Phenyl Sepharose HP hydrophobic interaction column (GE Lifesciences) with a gradient of 2.0 M to 0 M (NH₄)₂SO₄. AbfB fractions were pooled and subjected to size-exclusion chromatography on a 26/50 Superdex 75 column in 20 mM sodium acetate pH 5.0, 100 mM sodium chloride, 10 % glycerol.

Trichoderma reesei Cel7A was expressed and purified as previously described (37).

All enzymes were buffer-exchanged into 25 mM sodium citrate, pH 4.8, 50 mM sodium chloride using HiPrep desalting columns (GE Lifesciences, Piscataway, NJ). All enzymes were brought to a final concentration of 5 μ M.

Lignin Extraction: Switchgrass (*Panicum virgatum*) was collected from an established stand of Alamo variety grown in East Tennessee, air dried, and comminuted in a 1" knife mill to give material approximately 1-2" in length. Switchgrass fractionation was carried out by loading approximately 430 g of switchgrass into a perforated Teflon basket and placing the basket in a Hastelloy C276 flowthrough pressure reactor. The reactor was sealed and placed under vacuum for 30 minutes. A single-phase mixture of methyl isobutyl ketone (MIBK), ethanol (EtOH) and water (16/34/50 wt%) in the presence of 0.1M sulfuric acid as a catalyst was pulled into the reactor under vacuum and heated to 160°C. Additional solvent was pumped through the system into a collection tank for 120 minutes at a rate sufficient to generate approximately 7-8 liters of black liquor. Upon completion of the run, the solvent remaining in the reactor was carefully released into the collection tank and mixed with the black liquor collected during the run.

The black liquor was mixed with solid NaCl (10g/100 ml water contained in solvent mixture) in a separatory funnel, shaken, and allowed to stand for 30 minutes to generate aqueous and organic phases. The layers were separated and the organic layer was washed once with ~50% v/v water. The layers were separated and the organic layer was washed a second time with ~75% v/v water. Lignin was isolated from the organic fraction by solvent removal on the rotary evaporator. The resulting lignin residue was triturated with diethyl ether. After decanting the ether, the lignin was placed under vacuum. The trituration step was repeated as necessary to give a free flowing brown powder. Ethanol contained in the combined aqueous fractions from the washing was removed on the rotary evaporator to precipitate a second lignin fraction that was isolated by filtration through a double layer of filter paper in a Büchner funnel and dried under vacuum to give a free flowing brown powder.

Lignin thin films - Thin films of lignin were used as substrates for the QCM-D studies. The QCM resonators consist of 5 MHz-AT cut quartz crystals sensors between two conductive gold layers with an upper coating of SiO₂ (Q-Sense Style, Fil-Tech). The sensors were first cleaned with water and ethanol rinses followed by argon-ion plasma treatments. Cleaned QCM-D

sensors were then spin coated at 2000 rpm for 60 seconds with 100 μ l of 1 mg/ml of lignin dissolved in 9:1 dioxane:water.

Enzyme-Lignin Interactions Studied by QCM-D - A Q-Sense E4 (Biolin Scientific AB, Stockholm, Sweden) was used to study enzyme adsorption to lignin films deposited on the sensors. QCM-D measures both the change in frequency, Δf , and the change in dissipation, ΔD , of the quartz crystal. The temperature in our experiments was controlled to within ± 0.02 °C by a Peltier element within the QCM instrument.

For all binding experiments, bare quartz sensors were characterized in both air and buffer solution to measure their fundamental frequencies. Following this, the sensors were coated with lignin and characterized to measure the new fundamental frequencies, allowing the mass of the lignin films to be calculated. Odd harmonic overtones were collected and the third harmonic overtone was used to estimate the rates of adsorption.

Enzyme adsorption was monitored while flowing enzyme solution over the sensors for 25 minutes at a rate of 0.1 ml/min. Changes in dissipation were used to evaluate rigidity of the protein layer deposited on lignin surfaces. Changes in areal mass, Δm , were modeled using the Voigt viscoelastic model (38). The areal mass values obtained using the Voigt model generally agreed with the areal mass values obtained using the Sauerbrey equation, although the Sauerbrey equation did systematically under predict mass for about half of the proteins, which is a known limitation of the Sauerbrey model (39). The use of the Voigt viscoelastic model allowed for the estimation of the thickness for the adsorbed protein layer for *Aspergillus niger* BglI. The mass in all binding curves reached a plateau by 25 minutes, indicating saturation of binding. The binding capacity was therefore taken to be the areal mass value (ng/cm²) at 25 minutes.

Changes in frequency were fitted to an exponential decay function to model the initial enzyme adsorption rate as described by Turon et al. (40). The adsorption kinetics for nearly all proteins evaluated in this work did not fit to a single exponential. The use of a double-exponential equation improved the fit to the adsorption curve for many but not all of the proteins. Therefore, in order to provide a consistent method that could be applied to all

proteins, the initial adsorption rate for each enzyme to the lignin films was determined using the limiting slope method (Table 2). A range of greater than twenty fold is seen in the enzyme adsorption rates (Hz/min), with BSA as the fastest adsorbing protein and XynA the slowest.

Protein isoelectric point determination - The pI for each protein was determined using a pH 3-10 isoelectric focusing gel (IEF gel) (Life Technologies, Grand Island, NY.) with a Novex IEF Marker 3-10 standard. The loading buffer was 0.01% bromophenol blue, 0.01% methyl red and 10% glycerol. Electrophoresis conditions were 1 hour at 100V, 1 hour at 200V, and 0.5 hours at 500V. Proteins with more than one pI value, based on two or more bands in the IEF gel, were assigned a single pI value equal to the average of all determined pI values.

Analytical ultracentrifugation - The hydrodynamic properties of BglI were analyzed by analytical ultracentrifugation using sedimentation velocity. BglI was diluted to an OD₂₈₀ of 0.5 in 100 mM sodium chloride, 30 mM sodium acetate pH 5.0. The experiments were performed in a Beckman XL-A analytical ultracentrifuge (Beckman Coulter, CA) at 45,000 r.p.m. and 21 °C. The biophysical properties were determined by using Ultrascan III software with 2D spectrum analysis and a genetic algorithm (41).

Mass Spectrometry Analysis - BglI was supplied to Colorado State University Proteomics Facility and 1 μ l of the purified protein was mixed with 1 μ l of 2,5-dihydroxy benzoic acid (DHB, 10 mg/ml in 50% ACN, 0.1% TFA). The mixture was spotted on the MALDI target and allowed to air dry. The sample was analyzed by an Ultraflex-TOF/TOF mass spectrometer (Bruker Daltonics, Billerica, MA) in positive ion, reflector mode using a 25 kV accelerating voltage. External calibration was done using a peptide calibration mixture (4 to 6 peptides) on a spot adjacent to the sample. The raw data was processed in the FlexAnalysis software (version 3.3, Bruker Daltonics).

RESULTS

In this study we show that the software design program, Rosetta, can be used to predict protein adsorption to lignin by calculating the surface hydrophobicity. We also evaluated other physicochemical properties, such as protein size,

experimentally measured pI, total hydrophobic solvent accessible surface area (SASA), to determine the factors that influence enzyme binding to lignin. We select a set of proteins from families of industrially relevant cellulases or accessory biomass-degrading enzymes (Table 1). The enzymes have a diverse set of properties that allow a deeper investigation into the characteristics that drive adsorption to lignin. Bovine serum albumin (BSA) is included because it has demonstrated enhancements in enzymatic degradation of lignocellulosic biomass when added to the enzymatic mixture.

Analysis of solvent exposed hydrophobic patches – The simplest estimation of surface hydrophobicity of a protein structure is the hydrophobic solvent accessible surface area (SASA). The hydrophobic SASA of a protein can be a misleading metric as there is generally a positive correlation with the increasing size and thus increasing total surface. Evaluating the hydrophobic SASA as a percentage by normalizing by total SASA can give a more comparable metric of the relative amount of surface hydrophobicity, allowing for comparison of proteins of very different molecular weights.

Alternatively, the location of hydrophobic surface areas can be more informative than measuring surface hydrophobicity as location can be used to identify hydrophobic patches that can act as interaction sites. An example of a large hydrophobic patch identified on the surface of the *Trichoderma reesei* Cel7A CBM family 1 domain is shown (Figure 1 A and B). Here an algorithm that identifies and scores a protein based on the number and size of hydrophobic clusters, or patches, on the surface was used (17). The hydrophobic patch score increases exponentially with increasing patch size. This ensures that a larger protein such as AbfB with multiple small hydrophobic patches, will receive a more equivalent hydrophobic patch score to much smaller proteins such as XynII or XynA, which also have very small, negligible hydrophobic patch sizes but fewer of them due to protein size. A protein with large hydrophobic patches, such as BSA, will receive a high score that distinguishes it from the other proteins, highlighting the presence of possible interaction sites. The hydrophobic patches identified in BSA are known to bind hydrophobic ligands (23).

Comparing the hydrophobic patch score to the percentage of hydrophobic SASA shows the two do not have an apparent correlation (Figure 1C). BglI, for example, has the lowest percentage of hydrophobic SASA at 53%, just below two xylanases, XynA and XynII. Given that approximately half the SASA for BglI is hydrophobic, if the hydrophobic SASA were evenly distributed there would likely be no clustering of hydrophobic surface area that could act as interaction sites. However, BglI also has the highest hydrophobic patch score for all investigated proteins, resulting from the presence of four large hydrophobic clusters. The two metrics therefore allow for very different analyses of surface hydrophobicity.

Hydrophobic patch scores broken down by size of patches – The hydrophobic patch score by Jacek et al. was developed for the protein design software, Rosetta. The hydrophobic patch score was designed for the purpose of preventing the unintended formation of hydrophobic patches on the surface of computationally designed proteins, thus explicitly designing for enhanced solubility (17). As such, the objective function is mathematically designed to give large hydrophobic patches significantly higher scores.

The hydrophobic patches are placed into 50 Å² bins according to size. The smallest patch size seen in the examined set of proteins is 50 Å² or less, and the largest is close to 450 Å². The count of each hydrophobic patch size is given for the individual proteins in Figure 2A. The score increases exponentially per patch size, with a score of zero for patches of 50 Å², up to a score of 10.2 for patches of 450 Å², also shown in Figure 2A. The total hydrophobic patch score, as shown below x-axis in Figure 2C, is the sum of the scores for every identified patch on the protein.

AbfB and XynII have only small patches of 0-50 Å², receiving scores of zero, and 51-100 Å², receiving scores of 0.16 per patch. The resulting scores for AbfB and XynII are very similar despite the fact that AbfB is more than twice as large as XynII (Figure 2C and Table 1). On the other hand, the single patch found in BSA, sized 350 to 400 Å², accounts for a large portion of the total hydrophobic patch score (Figure 2B). The large patches, sized 400 to 450 Å² on the BglI dimer also contribute significantly to the total hydrophobic patch score.

Evaluating protein adsorption to lignin films – The interaction of the selected set of proteins with lignin was investigated using QCM-D. QCM-D allows for real-time monitoring of binding kinetics by measuring changes in the resonance frequency (Δf) that are proportional to changes in deposited mass on the sensor surface. After the protein injections, a change in resonance frequency was observed for all proteins, indicating enzyme adsorption to lignin films.

The Voigt viscoelastic model was used to estimate the change in deposited mass (ng/cm^2) from the measured Δf (Figure 3A). The total adsorbed mass for each protein was taken to be the adsorbed mass after 25 minutes, by which time all proteins had reached saturation of the lignin films. The total adsorbed mass at a point of saturation represents the binding capacity of the lignin for each protein. The proteins have greater than fifteen fold difference in total adsorbed mass, with BglI displaying the greatest adsorption capacity to lignin, and XynA displaying the least.

Hydrophobic patch scores correlate with protein-lignin adsorption parameters – We compare the adsorption capacity and the initial adsorption rates to the various physiochemical properties of each protein. The hydrophobic patch score shows a strong correlation with binding capacity (Figure 3B), with an R^2 of 0.94 for all investigated proteins. The percentage of hydrophobic SASA does not trend with binding capacity, which is not surprising since percent hydrophobic SASA does not trend with the hydrophobic patch score (Figure 3D). A strong correlation is also seen between the hydrophobic patch score and the initial rate of adsorption for all monomeric proteins, with an R^2 of 0.94 (Figure 3C). The seven monomeric proteins, ranging in size from 24 kDa to 66 kDa, display adsorption rates that trend with measured binding capacity, and show similar linear correlations with the hydrophobic patch scores. The large dimeric protein BglI, with a molecular weight of 235 kDa, shows a slower initial adsorption rate that does not trend with the high binding capacity or the hydrophobic patch score. As the hydrophobic patch score is designed to rank proteins based on the size and number of hydrophobic zones, these results suggest hydrophobic interaction describes a dominant component of interaction energy between the proteins and lignin films.

Interestingly, BSA and BglI display the largest patch sizes, and also exhibit significantly higher binding capacities to lignin surfaces, (Figure 2A and Table 2).

Molecular weight does not trend with binding capacity, verifying the observed correlations are not simply the result of the probability of finding larger patches, or more hydrophobicity on the surface of larger proteins. Specifically, AbfB has comparable hydrophobic patch score and binding capacity to both XynA and XynII, although the molecular weight of AbfB is approximately double the molecular weight of either endoxylanase (Tables 1 and 2 and Figure 3B). AbfB, Cel7A and BSA are comparable in molecular weight but display significantly different binding capacities and hydrophobic patch scores.

Aspergillus niger BglI binding agrees with location of hydrophobic patches – The crystal structure determined for *Aspergillus aculeatus* β -glucosidase 1 (BglI) reveals a dimeric complex in the asymmetric unit cell (PDB 4iib) (32). The dimeric interface buries 1450 \AA^2 of surface area and contains 25 hydrogen bonds. Further analysis using gel filtration chromatography show *A. aculeatus* BglI forms a dimer in solution as well. We investigate the oligomeric state of *Aspergillus niger* BglI using a native gel and sedimentation velocity analytical ultracentrifugation (AUC). The native gel shows no trace of the monomeric species, with a strong band for the dimer and a faint band for a higher-order oligomeric species (Figure 4). Sedimentation velocity results reveal a dominant presence of the dimeric species, with 95% of BglI appearing as a dimer (Table 3). The observed molecular weight of the native gel and AUC are higher than predicted based on sequence alone, thus the protein was further evaluated using mass spectrometry. The molecular weight was determined to be 117.5 kDa (Table 1) due to post-translational glycosylation. The dimeric structure for *A. aculeatus* BglI was therefore used to model *A. niger* BglI, including hydrophobic patch analysis.

The BglI was found to have the largest hydrophobic patch score for all proteins considered here, and also displayed the highest binding capacity for lignin surfaces. The Voigt viscoelastic model employed here to estimate deposited mass on lignin surfaces is also used to

estimate the thickness of deposited protein layers. The estimated thickness of the BglI layer on lignin was determined to be approximately 114 Å after 25 minutes of protein injection (Figure 5B). The BglI dimer forms an oblong structure with the identified hydrophobic patches located opposite each other on the long axis of the dimer. Interestingly, the distances between the hydrophobic patches are approximately 125 Å and 118 Å, in close agreement with the estimated thickness of the protein layer (Figure 5A). The shorter axis for the BglI dimer is approximately 68 Å, a distance that does not fit the measured thickness of the BglI protein layer thus precluding binding with the long, dimer axis parallel to lignin.

Protein surface charge shows no correlation with protein-lignin adsorption – Elevating pH has been shown to increase enzymatic saccharification of lignocellulose and decrease cellulase binding to lignin (42), although it is not clear how much of this effect is from changes in the lignin or the enzymes. We investigate the role of electrostatic interactions at constant pH by comparing protein surface charge, as measured by pI, to binding capacity on the lignin surfaces (Table 1). Proteins that display multiple bands on the IEF gel were given a single, average pI value for comparison to QCM-D-determined binding capacity. Our set of proteins includes enzymes with pI values ranging from 3.6 for AbfB to approximately 9 for XynII. Two endoxylanase enzymes from Glycoside Hydrolase family 11, XynA and XynII, have significantly different pI values (3.8 and 4.0 for XynA and 9 for XynII), but are nearly identical in molecular weights and hydrophobic patch scores.

Comparison between the pI for each protein and the binding capacity to lignin reveals no apparent correlation, with an R^2 of 0.06 (Figure 6). XynII and XynA have comparable binding capacity to lignin films. Conversely, BSA and Cel7A have similar pI values, with 4.6 for BSA and a range of 4.3 to 4.7 for Cel7A, yet the binding capacity of BSA for lignin films is more than twice that of Cel7A.

DISCUSSION

Enzymatic degradation of lignocellulosic biomass is a promising renewable source of liquid fuel provided cost reductions can be achieved. Cellulase preparation required to efficiently digest

sugars from lignocellulosic biomass remain a sizable portion of the total cost, prompting research investments in identifying avenues to improve cellulase efficiency and decrease costs. The loss of enzymatic activity due to the presence of lignin has therefore spurred considerable interest.

Multiple hypotheses regarding enzyme adsorption to lignin have been proposed, although the mechanism has remained elusive. Here, a systematic approach was used to investigate the role of hydrophobic interaction in enzyme-lignin adsorption. The hydrophobic patch score correlates surprisingly well with the measured enzyme adsorption to lignin. One protein, BglI, shows a lagging initial binding rate yet reaches the highest overall level of binding. BglI differs from the other proteins in two major facets; it forms a dimer in solution and has a pair of large distal hydrophobic patch regions. The other proteins are known to be monomeric (investigated by x-ray crystallography (28,30), gel-filtration chromatography (43-45), native polyacrylamide gel (46), and both analytical ultracentrifugation and gel-filtration chromatography (47)) and, excepting BSA, presented similar patterns of small, random hydrophobic patching on their surface (Figure 2C). Interaction energies are generally multifaceted, and the apparent dominance of the hydrophobic component could obscure other energetic contributions. Still, these results suggest that hydrophobic interaction accounts for much of the interaction energy between proteins and lignin.

Aspergillus niger BglI provides a unique opportunity to investigate a highly important cellulase enzyme that has been shown to preferentially adsorb to lignin when included in enzyme cocktails (6). BglI adsorption to lignin surfaces investigated here using QCM-D also shows higher adsorption capacity compared to other proteins, including BSA and *Trichoderma reesei* Cel7A. Interestingly, the distance from the lignin surface of the BglI layer is in agreement with the length of the BglI dimer if BglI adsorbs at either of the identified hydrophobic patches. Further, BglI has been shown to irreversibly adsorb to lignin yet still maintain activity (6). The hydrophobic patches identified here are far from the active site, allowing BglI to bind lignin while leaving the active sites available. β -glucosidase

enzymes act on soluble substrate, unlike other cellulase enzymes. Thus perhaps β -glucosidases, lacking a CBM domain, in fact benefit from adsorption to lignin, anchoring them near substrate yet not obscuring the active site.

Many cellulase enzymes are multi-domain proteins, with a catalytic domain defining the function and a carbohydrate-binding module (CBM) targeting the enzyme to substrate. Since CBMs concentrate enzymes onto substrates, they might also drive enzyme adsorption to lignin. Rahikainen et al. compared adsorption to lignin of the multi-domain *Trichoderma reesei* Cel7A to the isolated catalytic domain of Cel7A with CBM and linker removed. Using QCM-D, they found that the full-length Cel7A adsorbed to lignin films faster and to a greater extent than catalytic domain only (5).

Here, two proteins containing a Family 1 CBM are investigated, including *Trichoderma reesei* Cel7A. Hydrophobic patch analysis identifies the largest patch on the Cel7A CBM, not the catalytic domain, despite the fact that the CBM is much smaller. Hydrophobic patch analysis offers a possible explanation as to why the CBM increases adsorption to lignin for *T. reesei* Cel7A.

CBMs, divided into numerous families based on protein fold, display a variety of substrate specificities (47,48). In some cases a multivalent effect has been observed, where single cellulase enzymes contain multiple CBMs to increase association with target substrates (49,50). The presence of multiple CBMs may also be deleterious for enzymatic function depending on the substrate and the enzymatic mechanism, as seen with cellulosomes on pretreated biomass (51). Thus, evaluating the extent of enzyme adsorption to lignin for various CBM families and for enzymes containing multiple CBMs may be important for future cellulase engineering efforts.

Elevating pH is known to enhance enzymatic saccharification of lignocellulosic biomass and decrease enzyme adsorption to lignin (42,52). Here, the role of protein surface charge at a constant pH of 4.8 was investigated. Measured pI values did not show a correlation with enzyme adsorption to lignin. While it remains unclear whether altering pH has a larger effect on the enzyme or the lignin, protein surface charge does not identify which enzymes will preferentially adsorb. It is worth noting, however, that while

neither endoglucanase strongly adsorbed to lignin compared to the other proteins studied, XynII has a pI of approximately 9 and adsorbs more strongly to lignin compared to XynA with a pI of 3.9. Thus, engineering a protein to have a more positive surface charge may serve to attenuate lignin adsorption.

A model system of organosolv-extracted lignin from switchgrass was used to probe enzyme-lignin interactions independent of enzyme-cellulose interactions. Both the method of extraction as well as the plant source for lignin can result in different chemical properties that may alter enzyme-lignin interactions (53-55). Considering alternate sources of lignin and different extraction methods could build upon this work.

Understanding the mechanisms that drives enzyme adsorption to lignin promises to help engineering efforts to mitigate these undesired interactions. Detailed structural analysis affords a deeper understanding of enzyme-lignin interactions as well as the importance of various physicochemical properties and structural regions. The approach presented here offers the added benefit of identifying specific protein regions and sequence positions for future investigation.

References

1. Klein-Marcuschamer, D., Oleskowicz-Popiel, P., Simmons, B. A., and Blanch, H. W. (2012) The challenge of enzyme cost in the production of lignocellulosic biofuels. *Biotechnol Bioeng* **109**, 1083-1087
2. Nakagame, S., Chandra, R. P., Kadla, J. F., and Saddler, J. N. (2011) Enhancing the enzymatic hydrolysis of lignocellulosic biomass by increasing the carboxylic acid content of the associated lignin. *Biotechnol Bioeng* **108**, 538-548
3. Grabber, J. H. (2005) How do lignin composition, structure, and cross-linking affect degradability? A review of cell wall model studies. *Crop Sci* **45**, 820-831
4. Nakagame, S., Chandra, R. P., Kadla, J. F., and Saddler, J. N. (2011) The isolation, characterization and effect of lignin isolated from steam pretreated Douglas-fir on the enzymatic hydrolysis of cellulose. *Bioresour Technol* **102**, 4507-4517
5. Rahikainen, J. L., Martin-Sampedro, R., Heikkinen, H., Rovio, S., Marjamaa, K., Tamminen, T., Rojas, O. J., and Kruus, K. (2013) Inhibitory effect of lignin during cellulose bioconversion: the effect of lignin chemistry on non-productive enzyme adsorption. *Bioresour Technol* **133**, 270-278
6. Haven, M. O., and Jorgensen, H. (2013) Adsorption of beta-glucosidases in two commercial preparations onto pretreated biomass and lignin. *Biotechnol Biofuels* **6**, 165
7. Brethauer, S., Studer, M. H., Yang, B., and Wyman, C. E. (2011) The effect of bovine serum albumin on batch and continuous enzymatic cellulose hydrolysis mixed by stirring or shaking. *Bioresour Technol* **102**, 6295-6298
8. Yang, B., and Wyman, C. E. (2006) BSA treatment to enhance enzymatic hydrolysis of cellulose in lignin containing substrates. *Biotechnol Bioeng* **94**, 611-617
9. Zunszain, P. A., Ghuman, J., Komatsu, T., Tsuchida, E., and Curry, S. (2003) Crystal structural analysis of human serum albumin complexed with hemin and fatty acid. *BMC Struct Biol* **3**, 6
10. Lijnzaad, P., Berendsen, H. J., and Argos, P. (1996) Hydrophobic patches on the surfaces of protein structures. *Proteins* **25**, 389-397
11. Qing, Q., Yang, B., and Wyman, C. E. (2010) Impact of surfactants on pretreatment of corn stover. *Bioresour Technol* **101**, 5941-5951
12. Eriksson, T., Borjesson, J., and Tjerneld, F. (2002) Mechanism of surfactant effect in enzymatic hydrolysis of lignocellulose. *Enzyme Microb Tech* **31**, 353-364
13. Ballesteros, I., Oliva, J. M., Carrasco, J., Cabanas, A., Navarro, A. A., and Ballesteros, M. (1998) Effect of surfactants and zeolites on simultaneous saccharification and fermentation of steam-exploded poplar biomass to ethanol. *Appl Biochem Biotechnol* **70-72**, 369-381
14. Kaar, W. E., and Holtzapple, M. T. (1998) Benefits from tween during enzymic hydrolysis of corn stover. *Biotechnol Bioeng* **59**, 419-427
15. Kurakake, M., Ooshima, H., Kato, J., and Harano, Y. (1994) Pretreatment of Bagasse by Nonionic Surfactant for the Enzymatic-Hydrolysis. *Bioresour Technol* **49**, 247-251
16. Lijnzaad, P., Berendsen, H. J., and Argos, P. (1996) A method for detecting hydrophobic patches on protein surfaces. *Proteins* **26**, 192-203
17. Jacak, R., Leaver-Fay, A., and Kuhlman, B. (2012) Computational protein design with explicit consideration of surface hydrophobic patches. *Proteins* **80**, 825-838

18. Kuhlman, B., and Baker, D. (2000) Native protein sequences are close to optimal for their structures. *Proc Natl Acad Sci U S A* **97**, 10383-10388
19. Rohl, C. A., Strauss, C. E., Misura, K. M., and Baker, D. (2004) Protein structure prediction using Rosetta. *Methods Enzymol* **383**, 66-93
20. Willard, L., Ranjan, A., Zhang, H., Monzavi, H., Boyko, R. F., Sykes, B. D., and Wishart, D. S. (2003) VADAR: a web server for quantitative evaluation of protein structure quality. *Nucleic Acids Res* **31**, 3316-3319
21. Wilkins, M. R., Gasteiger, E., Bairoch, A., Sanchez, J. C., Williams, K. L., Appel, R. D., and Hochstrasser, D. F. (1999) Protein identification and analysis tools in the ExPASy server. *Methods Mol Biol* **112**, 531-552
22. Berman, H. M., Westbrook, J., Feng, Z., Gilliland, G., Bhat, T. N., Weissig, H., Shindyalov, I. N., and Bourne, P. E. (2000) The Protein Data Bank. *Nucleic Acids Res* **28**, 235-242
23. Bujacz, A. (2012) Structures of bovine, equine and leporine serum albumin. *Acta Crystallogr D Biol Crystallogr* **68**, 1278-1289
24. Baker, J. O., McCarley, J. R., Lovett, R., Yu, C. H., Adney, W. S., Rignall, T. R., Vinzant, T. B., Decker, S. R., Sakon, J., and Himmel, M. E. (2005) Catalytically enhanced endocellulase Cel5A from *Acidothermus cellulolyticus*. *Appl Biochem Biotechnol* **121-124**, 129-148
25. Divne, C., Stahlberg, J., Reinikainen, T., Ruohonen, L., Pettersson, G., Knowles, J. K., Teeri, T. T., and Jones, T. A. (1994) The three-dimensional crystal structure of the catalytic core of cellobiohydrolase I from *Trichoderma reesei*. *Science* **265**, 524-528
26. Kraulis, J., Clore, G. M., Nilges, M., Jones, T. A., Pettersson, G., Knowles, J., and Gronenborn, A. M. (1989) Determination of the three-dimensional solution structure of the C-terminal domain of cellobiohydrolase I from *Trichoderma reesei*. A study using nuclear magnetic resonance and hybrid distance geometry-dynamical simulated annealing. *Biochemistry* **28**, 7241-7257
27. Gruber, K., Klintschar, G., Hayn, M., Schlacher, A., Steiner, W., and Kratky, C. (1998) Thermophilic xylanase from *Thermomyces lanuginosus*: high-resolution X-ray structure and modeling studies. *Biochemistry* **37**, 13475-13485
28. Torronen, A., and Rouvinen, J. (1995) Structural comparison of two major endo-1,4-xylanases from *Trichoderma reesei*. *Biochemistry* **34**, 847-856
29. Hakulinen, N., Tenkanen, M., and Rouvinen, J. (2000) Three-dimensional structure of the catalytic core of acetylxyln esterase from *Trichoderma reesei*: insights into the deacetylation mechanism. *J Struct Biol* **132**, 180-190
30. Miyanaga, A., Koseki, T., Matsuzawa, H., Wakagi, T., Shoun, H., and Fushinobu, S. (2004) Crystal structure of a family 54 alpha-L-arabinofuranosidase reveals a novel carbohydrate-binding module that can bind arabinose. *J Biol Chem* **279**, 44907-44914
31. Kiefer, F., Arnold, K., Kunzli, M., Bordoli, L., and Schwede, T. (2009) The SWISS-MODEL Repository and associated resources. *Nucleic Acids Res* **37**, D387-392
32. Suzuki, K., Sumitani, J., Nam, Y. W., Nishimaki, T., Tani, S., Wakagi, T., Kawaguchi, T., and Fushinobu, S. (2013) Crystal structures of glycoside hydrolase family 3 beta-glucosidase 1 from *Aspergillus aculeatus*. *Biochem J* **452**, 211-221
33. Rastogi, P. A. (2000) MacVector. Integrated sequence analysis for the Macintosh. *Methods Mol Biol* **132**, 47-69

34. Selig, M. J., Knoshaug, E. P., Adney, W. S., Himmel, M. E., and Decker, S. R. (2008) Synergistic enhancement of cellobiohydrolase performance on pretreated corn stover by addition of xylanase and esterase activities. *Bioresour Technol* **99**, 4997-5005
35. Baker, J. O., McCarley, J. R., Lovett, R., Yu, C. H., Adney, W. S., Rignall, T. R., Vinzant, T. B., Decker, S. R., Sakon, J., and Himmel, M. E. (2005) Catalytically enhanced endocellulase Cel5A from *Acidothermus cellulolyticus*. *Appl Biochem Biotechnol* **121-124**, 129-148
36. Selig, M. J., Knoshaug, E. P., Adney, W. S., Himmel, M. E., and Decker, S. R. (2008) Synergistic enhancement of cellobiohydrolase performance on pretreated corn stover by addition of xylanase and esterase activities. *Bioresour Technol* **99**, 4997-5005
37. Jeoh, T., Michener, W., Himmel, M. E., Decker, S. R., and Adney, W. S. (2008) Implications of cellobiohydrolase glycosylation for use in biomass conversion. *Biotechnol Biofuels* **1**, 10
38. Voinova, M. V., Rodahl, M., Jonson, M., and Kasemo, B. (1999) Viscoelastic acoustic response of layered polymer films at fluid-solid interfaces: Continuum mechanics approach. *Phys Scripta* **59**, 391-396
39. Dutta, A. K., Nayak, A., and Belfort, G. (2008) Viscoelastic properties of adsorbed and cross-linked polypeptide and protein layers at a solid-liquid interface. *J Colloid Interface Sci* **324**, 55-60
40. Turon, X., Rojas, O. J., and Deinhammer, R. S. (2008) Enzymatic kinetics of cellulose hydrolysis: a QCM-D study. *Langmuir* **24**, 3880-3887
41. Scott, D. J., Harding, S. E., and Rowe, A. J. (2005) UltraScan - A Comprehensive Data Analysis Software Package for Analytical Ultracentrifugation Experiments. 210-230
42. Lou, H., Zhu, J. Y., Lan, T. Q., Lai, H., and Qiu, X. (2013) pH-Induced lignin surface modification to reduce nonspecific cellulase binding and enhance enzymatic saccharification of lignocelluloses. *ChemSusChem* **6**, 919-927
43. Pingali, S. V., O'Neill, H. M., McGaughey, J., Urban, V. S., Rempe, C. S., Petridis, L., Smith, J. C., Evans, B. R., and Heller, W. T. (2011) Small angle neutron scattering reveals pH-dependent conformational changes in *Trichoderma reesei* cellobiohydrolase I: implications for enzymatic activity. *J Biol Chem* **286**, 32801-32809
44. Sundberg, M., and Poutanen, K. (1991) Purification and Properties of 2-Acetylxylan Esterases of *Trichoderma-Reesei*. *Biotechnol Appl Bioc* **13**, 1-11
45. Sakon, J., Adney, W. S., Himmel, M. E., Thomas, S. R., and Karplus, P. A. (1996) Crystal structure of thermostable family 5 endocellulase E1 from *Acidothermus cellulolyticus* in complex with cellotetraose. *Biochemistry* **35**, 10648-10660
46. Shrivastava, S., Shukla, P., Deepalakshmi, P. D., and Mukhopadhyay, K. (2013) Characterization, cloning and functional expression of novel xylanase from *Thermomyces lanuginosus* SS-8 isolated from self-heating plant wreckage material. *World J Microbiol Biotechnol* **29**, 2407-2415
47. Lebowitz, J., Lewis, M. S., and Schuck, P. (2002) Modern analytical ultracentrifugation in protein science: a tutorial review. *Protein Sci* **11**, 2067-2079
48. Cuskin, F., Flint, J. E., Gloster, T. M., Morland, C., Basle, A., Henrissat, B., Coutinho, P. M., Strazzulli, A., Solovyova, A. S., Davies, G. J., and Gilbert, H. J. (2012) How nature

- can exploit nonspecific catalytic and carbohydrate binding modules to create enzymatic specificity. *Proc Natl Acad Sci U S A* **109**, 20889-20894
49. Boraston, A. B., Bolam, D. N., Gilbert, H. J., and Davies, G. J. (2004) Carbohydrate-binding modules: fine-tuning polysaccharide recognition. *Biochem J* **382**, 769-781
 50. Brunecky, R., Alahuhta, M., Xu, Q., Donohoe, B. S., Crowley, M. F., Kataeva, I. A., Yang, S. J., Resch, M. G., Adams, M. W., Lunin, V. V., Himmel, M. E., and Bomble, Y. J. (2013) Revealing nature's cellulase diversity: the digestion mechanism of *Caldicellulosiruptor bescii* CelA. *Science* **342**, 1513-1516
 51. Resch, M. G., Donohoe, B. S., Baker, J. O., Decker, S. R., Bayer, E. A., Beckham, G. T., and Himmel, M. E. (2013) Fungal cellulases and complexed cellulosomal enzymes exhibit synergistic mechanisms in cellulose deconstruction. *Energ Environ Sci* **6**, 1858-1867
 52. Rahikainen, J. L., Evans, J. D., Mikander, S., Kalliola, A., Puranen, T., Tamminen, T., Marjamaa, K., and Kruus, K. (2013) Cellulase-lignin interactions-The role of carbohydrate-binding module and pH in non-productive binding. *Enzyme Microb Tech* **53**, 315-321
 53. El Hage, R., Brosse, N., Chrusciel, L., Sanchez, C., Sannigrahi, P., and Ragauskas, A. (2009) Characterization of milled wood lignin and ethanol organosolv lignin from miscanthus. *Polym Degrad Stabil* **94**, 1632-1638
 54. El Hage, R., Brosse, N., Sannigrahi, P., and Ragauskas, A. (2010) Effects of process severity on the chemical structure of Miscanthus ethanol organosolv lignin. *Polym Degrad Stabil* **95**, 997-1003
 55. Erdtman, H. (1972) Lignins: Occurrence, formation, structure and reactions, K. V. Sarkanen and C. H. Ludwig, Eds., John Wiley & Sons, Inc., New York. *J Polymer Sci Part B: Polymer Letters* **10**, 228-230

Footnotes

This work was supported by the U.S. Department of Energy under Contract No. DE-AC36-08GO28308 with the National Renewable Energy Laboratory. Funding for the work was provided by the DOE Office of Energy Efficiency and Renewable Energy, Bioenergy Technologies Office.

This work was also supported by the Center for Direct Catalytic Conversion of Biomass to Biofuels (C3Bio), an Energy Frontier Research Center funded by the U.S. Department of Energy, Office of Science, Office of Basic Energy Sciences under Award Number DE-SC0000997.

Partial contribution of NIST, an agency of the US government; not subject to copyright in the United States. Certain commercial equipment, instruments, or materials are identified in this document. Such identification implies neither recommendation nor endorsement by the National Institute of Standards and Technology, nor that the products identified are necessarily the best available for the purpose.

Figure 1: The total hydrophobic solvent accessible surface area does not determine the presence of hydrophobic clusters. (A) The Family 1 Carbohydrate Binding Module (CBM1, PDB 1cbh) from *Trichoderma reesei* Cel7A (GH7) is shown in sphere representation, with polar atoms colored red (oxygen) and blue (nitrogen), and non-polar atoms shown in grey (carbon). Hydrogen atoms are shown in white. Non-polar atoms from the largest hydrophobic cluster found on CBM1 are shown in orange. (B) Cartoon and surface representation of the CBM1 shown with the identified hydrophobic cluster highlighted in orange. (C) Hydrophobic patch scores are plotted against the percentage of hydrophobic SASA to show the lack of correlation between the percentage of hydrophobic SASA and the presence of large solvent exposed hydrophobic patches as identified by the hydrophobic patch score.

Figure 2. The hydrophobic patch score broken down by the number and size of identified patches for each enzyme suggests a minimum patch size for preferential lignin adsorption. (A) The individual hydrophobic patch score for each bin size is shown with red dots (right y-axis). The count for each hydrophobic patch size found in the investigated set of proteins is shown with bars (left y-axis). (B) A surface representation of BSA with two of the four largest identified hydrophobic patches highlighted in orange and side-chains shown in stick representation. (C) The hydrophobic patch scores for each protein are listed in brackets under the protein name under the x-axis. The count for each hydrophobic patch size is broken down for each protein. The patch sizes are binned by \AA^2 of solvent accessible surface area. Larger patches ($>350 \text{ \AA}^2$ of SASA) are only observed on *Aspergillus niger* BglI and BSA. Since the score increases exponentially for each bin size, the larger hydrophobic patch scores seen in BglI and BSA are explained by the presence of larger hydrophobic patches.

Figure 3. A correlation exists between enzyme-lignin adsorption parameters and the number and size of hydrophobic patches on the surface of enzymes. (A) QCM-D adsorption curves for a set of eight enzymes are shown. (B) A linear correlation exists between the hydrophobic patch score for each protein and the total change in adsorbed mass on the lignin surfaces. The error bars are so small relative to the differences in areal mass that they are not visible in the graph. The error bars for areal mass for each protein are given in Table 2. (C) A correlation is also seen for the initial adsorption rate for the seven monomeric proteins, determined by the slope of the initial linear portion of the adsorption curves, and the hydrophobic patch score. The initial rate of adsorption for BglI dimer unexpectedly lags the high adsorption capacity and the large hydrophobic patch score. This data point is shown but not included in the trend line. (D) The percentage of hydrophobic SASA does not correlate with the binding capacity as determined by the total adsorbed mass. The error bars for total adsorbed mass are given in Table 2 as they are so small relative to the differences in adsorbed mass that they are not visible in the graph.

Figure 4. *Aspergillus niger* BglI is a homodimer. Native PAGE of *A. niger* BglI. 30 μg of BglI was run on a 2-12% Native PAGE (Life Technologies) and stained with SimplyBlue protein stain. The protein molecular weight aligns as a dimer, with no detectable band for monomeric species. There is, however, a band running at a higher molecular weight that may be a tetramer or higher-order oligomeric species.

Figure 5. The distance of the dimeric structure between hydrophobic patches on *Aspergillus niger* BglI agrees with the thickness of the deposited protein layer as evaluated with QCM-D. (A) The modeled BglI dimer is shown in cartoon and surface representation with the 4 largest hydrophobic patches highlighted with orange spheres. Distances between the hydrophobic patches (125 and 118 \AA) are shown with arrows, and the monomer thickness across the short axis is shown below (68 \AA). (B) The estimated thickness of the BglI protein layer on the lignin surface is shown. The first three minutes is the flow of buffer only, followed by 25 minutes of protein injection.

Figure 6. There is no correlation between the pI and measured binding capacity to lignin surfaces for the investigated proteins. pI values were averaged for enzymes with multiple bands in the IEF gels in order to

Hydrophobic clusters predict level of enzyme adsorption to lignin.

obtain single pI values to compare to adsorbed mass values. The error bars for total adsorbed mass for each protein are given in Table 2 as they are so small relative to the differences in total adsorbed mass that they are not visible in the graph.

Table 1. Physical characteristics for the set of enzymes selected for *in silico* structure-based surface analysis and biophysical characterization using QCM-D.

Protein	Organism	Domain Architecture	pI	MW (kDa)	% SASA _{Hydrophobic}	Hydrophobic Patch Score
β -glucosidase (Bgl1)	<i>Aspergillus niger</i>	GH3	4.2	93.3 [117.5]*	53.0%**	45.9**
Serum Albumin	Bovine	BSA	4.6	66.5	60.5%	34.9
Cellobiohydrolase (Cel7A)	<i>Trichoderma reesei</i>	GH7 - CBM1	4.3	54.1	59.1%	13.3
Acetyl Xylan Esterase (Axe1)	<i>Trichoderma reesei</i>	Axe1 - CBM1	6.8, 6.9, 7.1 , 7.4	30.8	70.7%	9.1
Endocellulase (E1)	<i>Acidothermus cellulolyticus</i>	GH5	5.2	40.1	60.1%	7.7
Endoxylanase (XynA)	<i>Thermomyces lanuginosus</i>	GH11	3.8, 4.0	24.4	54.1%	2.7
Arabinofuranosidase (AbfB)	<i>Aspergillus niger</i>	GH54	3.6, 3.8	52.5	57.0%	1.9
Endoxylanase (XynII)	<i>Trichoderma reesei</i>	GH11	9	24.2	54.6%	0.8

* Molecular weight for Bgl1 shown in brackets was determined by Mass Spectrometry. Molecular weights for Bgl1 are for the monomeric species.

** SASA calculations and Hydrophobic Patch Score for Bgl1 are for the dimeric species.

Major bands are shown in bold and underlined

Table 2. QCM-D measured adsorption parameters for proteins on lignin surfaces. Duplicate runs were performed for each enzyme, and the additional rates of adsorption and adsorbed mass after twenty-five minutes of protein injection are shown in brackets.

	Adsorbed Mass (ng/cm ²)	Std. Dev. Δ Mass	Rate of Adsorption (Hz/min)	Std. Dev. Rate
BglI	1155.6 [1170.6]	10.6	8.2 [6.8]	1.0
BSA	643.3 [631.7]	8.2	21.3 [21.2]	0.1
Cel7A	294.6 [285.8]	6.2	8.3 [6.3]	1.4
Axe1	263.4 [245.3]	12.8	10.1 [11.7]	1.1
E1	193.2 [192.5]	0.5	3.9 [3.8]	0.1
AbfB	170.5 [191.5]	14.8	2.6 [1.5]	0.8
XynII	172.2 [162.1]	7.1	1.5 [2.2]	0.5
XynA	69.7 [69.4]	0.2	1.0 [0.6]	0.3

Table 3. Sedimentation velocity analysis for *Aspergillus niger* BglI. Sedimentation coefficient distribution determined by van Holde Weishet analysis using Ultrascan III. BglI was diluted to an OD280 of 0.5 in 100 mM NaCl, 30 mM sodium acetate at pH 5.0 and centrifuged at 50k rpm. The sedimentation velocity data shown was determined using Ultrascan III software using 2-D spectrum analysis and genetic algorithm. AUC data suggests that BglI is primarily a dimeric species with a molecular weight of 235 kDa and also contains 5% oligomers or other contaminants.

Molec. Wt.	S Apparent	S 20,W	D Apparent	D 20,W	f/f ₀	Concentration
2.35E+05	1.11E-12	1.08E-12	4.03E-07	4.04E-07	1.30E+00	0.55829 [94.68%]
1.58E+06	1.29E-12	1.25E-12	6.92E-08	6.93E-08	4.03E+00	0.0069564 [1.18%]
2.32E+05	1.58E-12	1.53E-12	5.76E-07	5.77E-07	9.17E-01	0.02439 [4.14%]

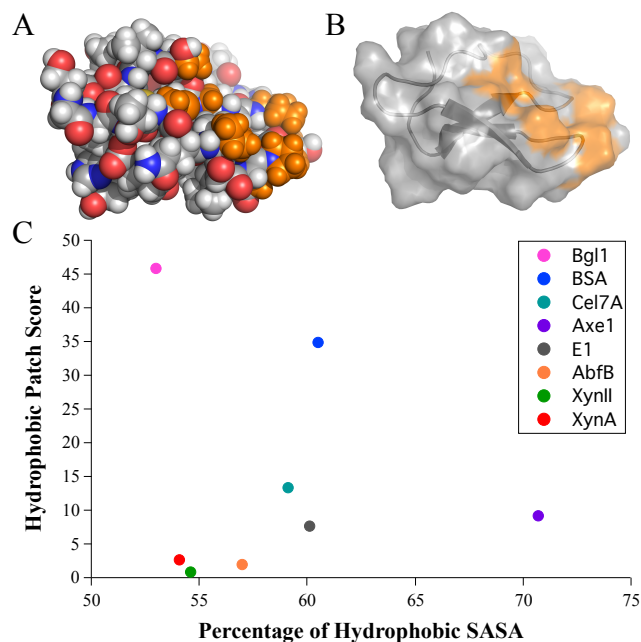


Figure 1.

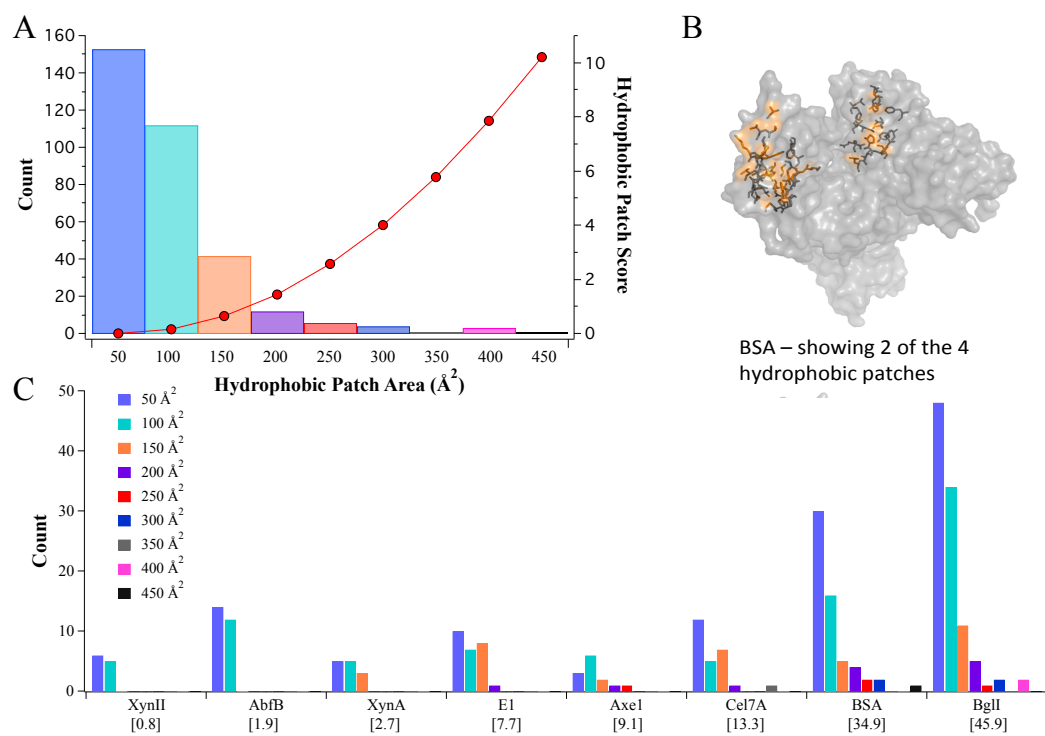


Figure 2.

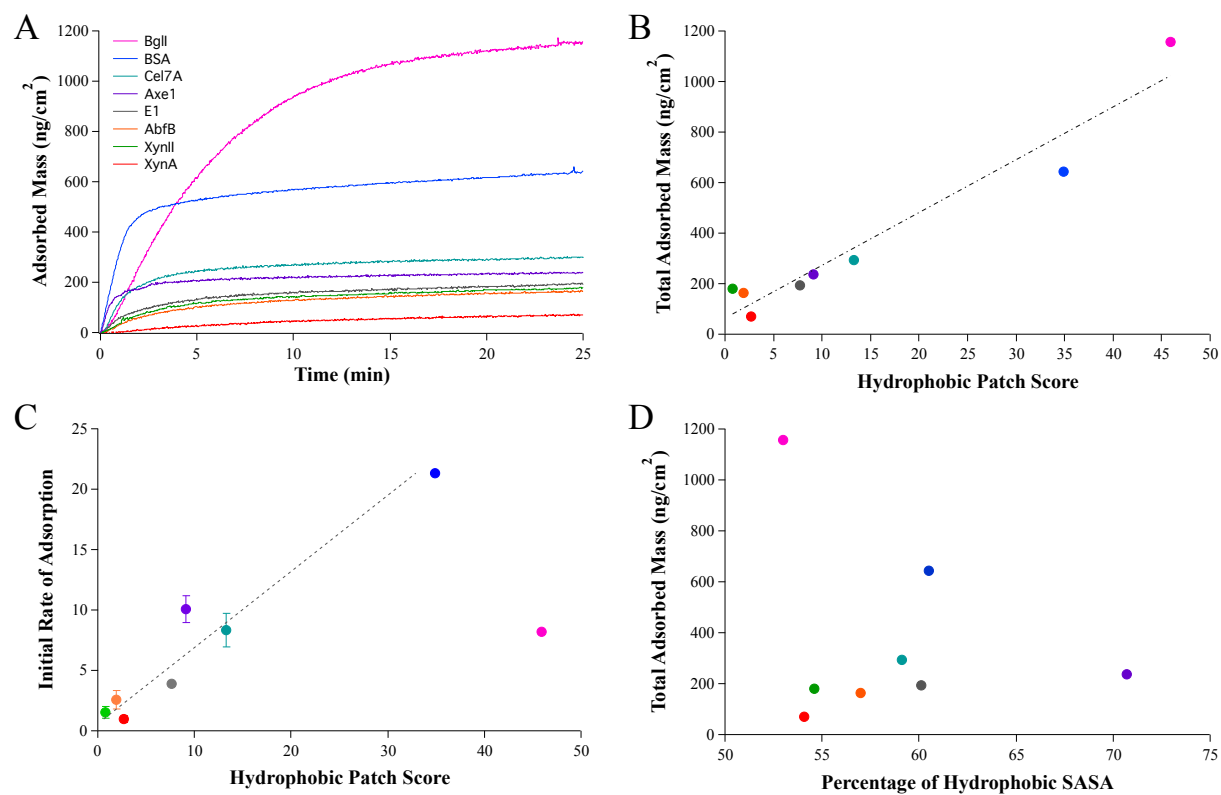


Figure 3.

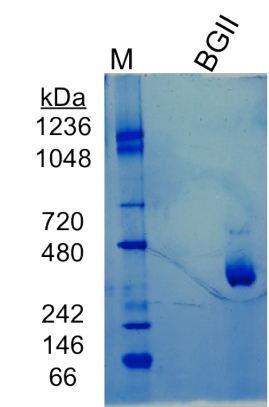


Figure 4.

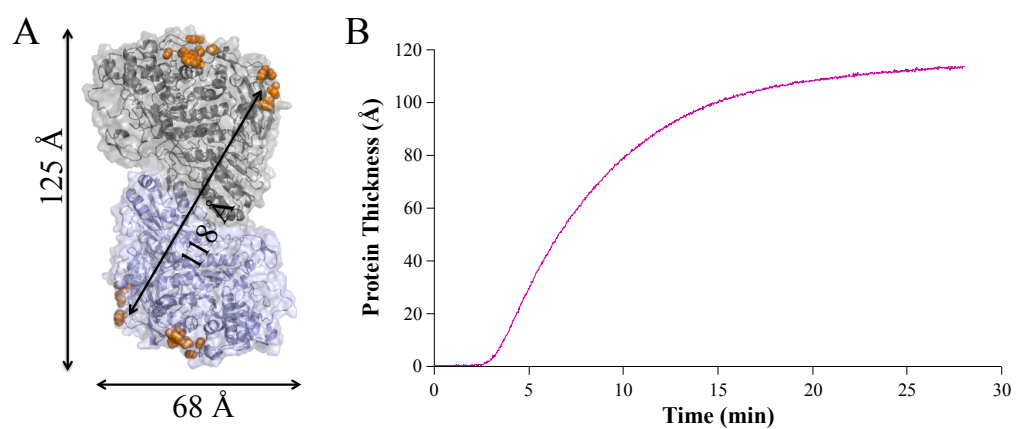


Figure 5.

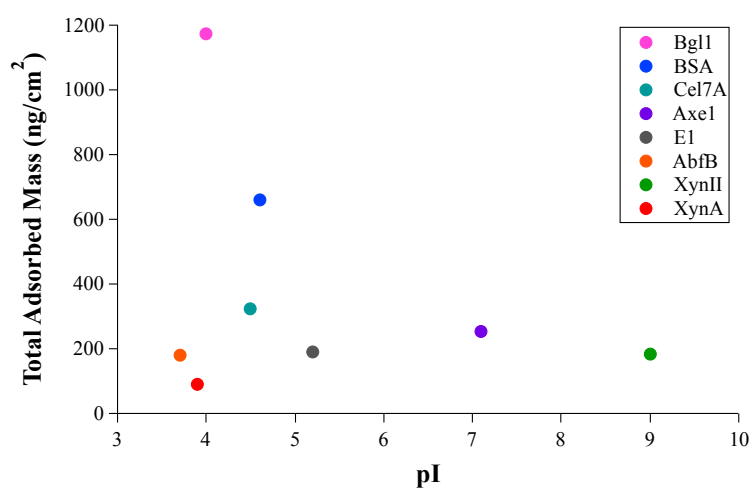


Figure 6.